

Leveraging *Sparse* LiDAR for RAFT-Stereo: A Depth Pre-Fill Perspective

Jinsu Yoo, Sooyoung Jeon, Zanming Huang, Tai-Yu Pan, Wei-Lun Chao
The Ohio State University

Abstract

We investigate LiDAR guidance within the RAFT-Stereo framework, aiming to improve stereo matching accuracy by injecting precise LiDAR depth into the initial disparity map. We find that the effectiveness of LiDAR guidance drastically degrades when the LiDAR points become sparse (*e.g.*, a few hundred points per frame), and we offer a novel explanation from a signal processing perspective. This insight leads to a surprisingly simple solution that enables LiDAR-guided RAFT-Stereo to thrive: pre-filling the sparse initial disparity map with interpolation. Interestingly, we find that pre-filling is also effective when injecting LiDAR depth into image features via early fusion, but for a fundamentally different reason, necessitating a distinct pre-filling approach. By combining both solutions, the proposed **Guided RAFT-Stereo (GRAFT-Stereo)** significantly outperforms existing LiDAR-guided methods under sparse LiDAR conditions across various datasets. We hope this study inspires more effective LiDAR-guided stereo methods.¹

1 Introduction

This paper originated from the need to improve stereo depth estimation, particularly for RAFT-Stereo [1]. In recent years, RAFT-Stereo variants [1, 2, 3, 4] have demonstrated excellent performance in estimating pixel disparity between two parallel images. Compared to convolutional neural network-based [5, 6, 7] and Transformer-based methods [8, 9], RAFT-Stereo has a distinctive advantage: *it supports anytime prediction*. By utilizing recurrent neural networks for iterative refinement, RAFT-Stereo allows users to trade speed for accuracy, offering faster but less accurate depth when inference time is constrained, or allowing more iterations for better accuracy. However, like all stereo matching methods, RAFT-Stereo often struggles in outdoor scenes with complex content and distant ranges. Bridging the gap between estimated and actual depth in such scenes remains an open challenge.

LiDAR-guided stereo offers a promising solution to this challenge by *leveraging sparse yet more accurate LiDAR depth to improve dense stereo depth prediction*. Previous work has primarily relied on convolutional neural networks [10, 11, 12]. In this paper, we explore how to integrate LiDAR inputs into the RAFT-Stereo framework. *Our goal is to develop a principled approach that introduces minimal changes to RAFT-Stereo, preserving its inherent strengths.*

We first investigate where to inject LiDAR depth. We identify the *initial disparity map* in RAFT-Stereo as an ideal candidate, as it is designed to process disparity values rather than features. In essence, RAFT-Stereo iteratively refines this map, improving the disparity estimate with each update. This led us to hypothesize that LiDAR depth, once converted to disparity, could be seamlessly injected into the map without the need for additional encoding [13]. Our initial, albeit vanilla, attempt yielded promising results. Under the standard stereo-LiDAR fusion setup with 64-beam LiDAR points [11, 12], replacing the default zero initial disparity with LiDAR-derived values effectively reduces the average disparity error to 0.317 for RAFT-Stereo, compared to 0.300 for the state-of-the-art (SotA) LiDAR-guided method [12].

¹Project page: <https://jinsuyoo.info/grafft-stereo>.

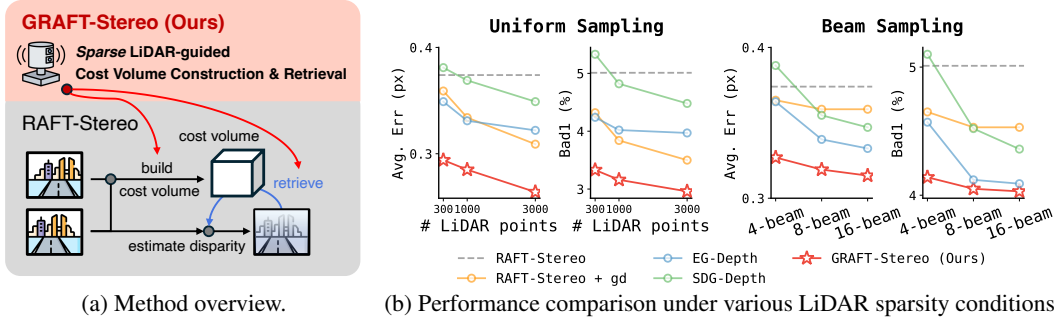


Figure 1: **Overview of GRAFT-Stereo.** (a): **GRAFT-Stereo** effectively integrates very sparse LiDAR points with minimal modifications to **RAFT-Stereo** [1]. (b): **GRAFT-Stereo** achieves a substantial reduction in disparity error on the KITTI benchmark [14] across various LiDAR sparsity conditions, surpassing the SotA LiDAR-guided stereo methods, **EG-Depth** [11] and **SDG-Depth** [12]. gd: naive LiDAR-guidance; Avg. Err: average disparity error over all pixels; Bad1: percentage of pixels with a disparity error greater than 1.0 pixel.

However, assuming access to a 64-beam LiDAR is often impractical, as such sensors cost over ten thousand dollars [15], contradicting stereo depth’s key advantage: affordability. Ideally, we seek to leverage LiDAR input with minimal added cost, recognizing that only limited points may be available in practice. Unfortunately, as shown in Fig. 1b and Fig. 3, the error rate of *vanilla LiDAR-guided RAFT-Stereo* increases sharply as the number of LiDAR points decreases.

To better understand this limitation, we conduct a detailed analysis and find that the performance drop is not solely due to the reduced point count but also to the *internal mechanics of RAFT-Stereo*, which unintentionally suppresses the impact of LiDAR guidance. Specifically, RAFT-Stereo uses the (initial/previous) disparity map to index cost volume features during refinement. In extremely sparse settings, most pixels are initialized with zero disparity, while only a few receive accurate values from LiDAR. As a result, the features retrieved from these accurate disparities appear as high-frequency outliers relative to the dominant zero-disparity initialization and are subsequently attenuated by the recurrent convolution operations.

Building on this insight, we propose a simple yet highly effective solution: *pre-filling the LiDAR-missing pixels* in the initial disparity map. Remarkably, by applying a purely image-processing-based interpolation method [16] to densify extremely sparse disparities (e.g., 300 points), the resulting LiDAR-guided RAFT-Stereo surpasses its counterpart that uses 64-beam LiDAR without pre-filling.

We further investigate alternative locations within RAFT-Stereo for incorporating LiDAR information. Notably, appending the 3D coordinates of each LiDAR point to the RGB values of the corresponding pixels in both images proves effective, as it explicitly reinforces stereo correspondence. For this form of LiDAR guidance, pre-filling LiDAR-missing pixels remains beneficial. However, it demands a more advanced approach to provide more accurate depth estimates than simple interpolation.

By integrating both forms of LiDAR guidance with their respective pre-filling strategies, our proposed **Guided RAFT-Stereo (GRAFT-Stereo)** achieves SotA stereo matching performance under extremely sparse LiDAR conditions (see Fig. 1). Extensive experiments on three outdoor datasets—KITTI Depth Completion [14], VKITTI2 [17], and MS2 [18]—consistently validate its effectiveness.

To summarize, our main contributions are as follows:

- We examine RAFT-Stereo’s effectiveness and limitations as a LiDAR-guidance stereo framework.
- We propose **GRAFT-Stereo**, a method that enables RAFT-Stereo to effectively exploit extremely sparse LiDAR input via a depth pre-filling approach.
- We validate **GRAFT-Stereo** through extensive experiments on three outdoor datasets, demonstrating SotA performance under sparse LiDAR conditions.

2 Related Work

Stereo matching. Traditional stereo matching methods focused on handcrafted features and prior modeling [19, 20, 21, 22, 23], whereas deep learning has since transformed the field [24, 25, 26, 27, 28, 29, 30, 31, 32, 33, 34]. Recent methods can be broadly categorized into three groups: CNN-based, Transformer-based, and iterative approaches. CNN-based methods [5, 6, 35, 7] construct and aggregate a cost volume, typically using 3D convolutions—an approach achieving high accuracy

but is computationally intensive. Transformer-based methods [8, 9], inspired by the success of Vision Transformers [36], replace conventional cost volume processing with optimal transport and attention mechanisms. Iterative methods [1, 2, 4, 37, 3, 38, 39], drawing from the RAFT recurrent flow estimation framework [40], process cost volumes through iterative feature retrieval, offering higher efficiency and enabling anytime prediction. Despite these advances, estimating dense depth in complex scenarios—like outdoor driving and diverse weather—remains challenging.

LiDAR-guided stereo. To overcome the limitations of standard stereo matching, guided stereo incorporates additional reliable depth measurements, typically from a LiDAR sensor [41, 42, 10, 43, 44, 45, 32]. Prior work has explored various integration strategies, including cost volume adjustment with sparse depth input [46, 47], as well as fusion at the input and feature levels [48, 49, 11, 12]. Aligned with this direction, we aim to enhance dense depth estimation using sparse LiDAR guidance. We focus on RAFT-Stereo [1] for its recent success, architectural modularity, and iterative refinement capability, and examine its compatibility with extremely sparse LiDAR input (*e.g.*, 300 points), targeting cost-efficient deployment in real-world scenarios.

Depth completion. Our work is inspired by depth completion, which estimates dense depth from *monocular* images and sparse LiDAR input [50, 51]. Prior efforts have primarily focused on leveraging sparse depth through feature extraction [52, 53, 54] or spatial propagation [55, 56, 57, 58], with pre-filling strategies also being explored [59]. In this paper, we systematically analyze RAFT-Stereo’s cost volume retrieval mechanism, identify its core limitation in utilizing LiDAR guidance, and propose pre-filling as a *simple yet highly effective* solution.

3 Background: Stereo Matching for Disparity Estimation and RAFT-Stereo

Given a pair of rectified images I_l and I_r from parallel cameras, **stereo matching** estimates the horizontal pixel disparity by identifying corresponding pixels across the two images. Let $D(h, w)$ denote the disparity at pixel (h, w) in the left image I_l , where h and w represent the vertical and horizontal coordinates, respectively. Ideally, $I_l(h, w)$ and $I_r(h, w - D(h, w))$ correspond to the same 3D point in the scene. The disparity map D can be converted into a depth map Z using the known focal length f and camera baseline b (*i.e.*, the distance between the cameras), as $Z(h, w) = \frac{f \cdot b}{D(h, w)}$.

Traditional stereo methods typically construct a 3D cost volume C that encodes pixel-wise correspondences along horizontal scanlines, where $C(h, w, w')$ represents the similarity between pixels $I_l(h, w)$ and $I_r(h, w')$. Given a reliable cost volume, the disparity at pixel (h, w) can be estimated as $D(h, w) = w - \arg \max_{w'} C(h, w, w')$. However, the cost volume is often degraded by challenging conditions such as lighting variations, occlusions, or textureless regions. To mitigate these issues, standard approaches apply computationally intensive 3D convolutions to denoise the cost volume, often incorporating smoothness priors to regularize the final disparity estimates.

RAFT-Stereo [1] bypasses 3D convolutions by iteratively refining disparity estimates. At each step, it extracts a local region of the 3D cost volume C centered on the current estimate D , and refines the disparity using recurrent 2D convolutional networks. This approach regularizes the cost volume selectively—only where needed—yielding both accuracy and efficiency. Let H and W denote the height and width of the image, respectively. Conceptually, a local region $S \in \mathbb{R}^{H \times W \times (2K+1)}$ can be constructed by retrieving the $2K+1$ cost values centered at the current estimate, *i.e.*, at $w' = w - D(h, w)$ for each pixel (h, w) :

$$S(h, w, k) = C(h, w, w - D(h, w) + k), k \in [-K, K]. \quad (1)$$

The resulting S can be processed by 2D convolutions, treating the 3rd dimension as the channel axis.

Without loss of generality, a RAFT-Stereo model can be implemented as follows. Given I_l and I_r , it first extracts feature maps X_l and X_r using a shared 2D CNN backbone (*e.g.*, ResNet [60]). Each feature map is of size $H \times W \times J$, where J is the feature dimensionality. Next, a 3D correlation volume is constructed by:

$$C(h, w, w') = \sum_j X_l(h, w, j) \cdot X_r(h, w', j). \quad (2)$$

Then, starting from an initial disparity map $D^{(0)}$ (typically set to zero), the model iteratively refines the estimate. At iteration t , it retrieves $S^{(t)}$ from C based on the current estimate $D^{(t-1)}$, and applies

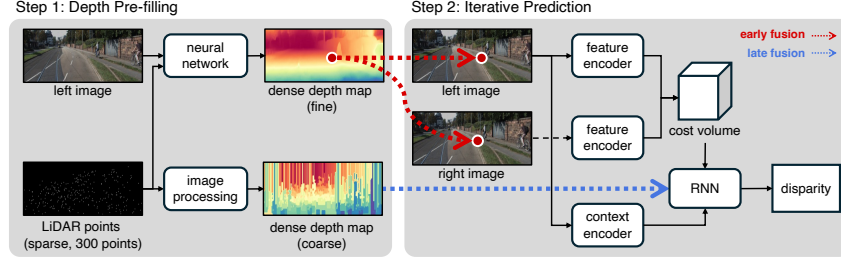


Figure 2: **Illustration of the proposed GRAFT-Stereo.** Given extremely sparse LiDAR points (*e.g.*, 300 points), we systematically identify two complementary strategies to incorporate the LiDAR information into RAFT-Stereo: early fusion and late fusion. Our analysis reveals that *depth pre-filling* is the key to leveraging extremely sparse LiDAR guidance for effective stereo matching.

a recurrent 2D CNN to predict a residual disparity $\Delta^{(t)}$. The estimate is then updated as:

$$D^{(t)} = D^{(t-1)} + \Delta^{(t)}.$$

During training, the model is optimized to minimize the difference between $D^{(t)}$ and the ground-truth disparity map D^* , for all $t \in [1, T]$, where T is the maximum number of iterations. At test time, the model supports anytime prediction: each intermediate output $D^{(t)}$ serves as a valid estimate, with higher t generally yielding greater accuracy.

4 Setup, Goal, and Preliminary Results

Like other stereo methods, RAFT-Stereo faces challenges in outdoor environments with complex scenes and wide depth variation. This paper investigates how to leverage sparse yet accurate LiDAR depth to enhance dense stereo matching. Our study follows a systematic, step-by-step analysis, beginning with a clear outline of the setup and goals.

4.1 Experiment setup

Datasets. We focus on stereo-LiDAR fusion in outdoor settings and primarily evaluate on the KITTI Depth Completion dataset [14], which consists of 42,949 training and 3,426 validation stereo image pairs with corresponding 64-beam LiDAR scans from driving scenes. Each image has a resolution of 375×1242 . Ground-truth depth is semi-densified by aggregating LiDAR points from neighboring frames, yielding approximately 100k valid points per frame. Following previous works [11, 12], we report results on the validation set. We further demonstrate the effectiveness of our method on the VKITTI2 [17] and MS2 [18] datasets.

Evaluation metrics. To evaluate disparity estimates, we compute error rates: the percentage of pixels with a disparity error greater than one (*i.e.*, Bad1) or two (*i.e.*, Bad2) pixels from the ground-truth disparity map. We also report the average disparity error over all pixels. The maximum disparity is set to 192. For depth evaluation, we report both the mean absolute error (MAE) and the root mean squared error (RMSE) from the ground-truth semi-dense depth map in millimeters (mm).

Implementations. We follow the official implementation of RAFT-Stereo [1], including objective functions and hyperparameters. We evaluate on $t = 32$ during inference, unless stated otherwise. See the supplementary material for details.

4.2 Goal: affordable settings with limited points

We aim to investigate LiDAR-guided RAFT-Stereo with minimal additional cost. As discussed in Sec. 1, a 64-beam LiDAR sensor—capable of producing over 10,000 points per frame—is prohibitively expensive for many applications. Thus, we focus on leveraging much sparser LiDAR guidance that simulates the output of lower-cost sensors. We consider two settings: (1) uniformly subsampling the ground-truth semi-dense depth map, following [47]; and (2) synthesizing a reduced-beam LiDAR response from the original 64-beam data, inspired by [61]. In extreme cases, a single LiDAR scan may contain only a few hundred points—orders of magnitude fewer than the number of pixels per image (*e.g.*, over 400k in the KITTI dataset).

Table 1: **Vanilla LiDAR guidance for RAFT-based stereo methods with 64-beam sensors.** Iterative refinement-based methods show great potential for LiDAR guidance even *without architectural changes*. SDG-Depth [12] is the SotA LiDAR-guided stereo method.

Method	Guidance	Bad1 (%)	Bad2 (%)	Avg. Err. (px)
RAFT-Stereo [1]	×	5.01	0.41	0.374
RAFT-Stereo [1]	64-beam	4.12	0.37	0.317
Selective-RAFT [3]	×	5.00	0.39	0.379
Selective-RAFT [3]	64-beam	4.05	0.36	0.318
SDG-Depth [12]	64-beam	3.60	0.36	0.300

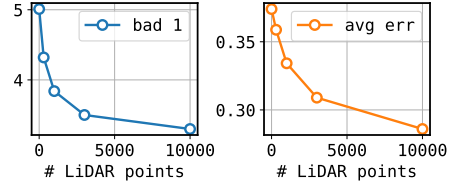


Figure 3: **Performance of RAFT-Stereo with different numbers of LiDAR points.** The disparity error increases drastically as the number of LiDAR guidance points reduces.

4.3 Preliminary results

Where to inject LiDAR points? The modular design of RAFT-Stereo allows LiDAR information to be integrated at different stages. In addition to early fusion in image space and intermediate fusion in feature space, *RAFT-Stereo offers a unique late fusion opportunity via its initial disparity map*. This map is typically initialized to zero, but its iterative refinement process suggests that a more accurate initialization could improve performance. This insight is supported by recent work in optical flow [62], which shows that better initialization enhances RAFT-based results. Motivated by this, we explore initializing RAFT-Stereo’s disparity map using sparse LiDAR depth.

Results with 64-beam LiDAR. We begin with the standard dense LiDAR-guided stereo setting [11, 12]. We inject LiDAR-derived disparities into the corresponding pixel locations of the initial map, and re-train RAFT-Stereo [1] and the recently proposed variant Selective-RAFT [3]. Surprisingly, this simple strategy already yields performance comparable to the SotA LiDAR-guided stereo method [12], underscoring the strong compatibility of RAFT-Stereo with LiDAR guidance (Table 1).

Results with fewer LiDAR points. We next investigate the impact of injecting fewer points into the initial map. Separate models are trained under varying LiDAR sparsity. As shown in Fig. 3, the performance gains from LiDAR guidance drop sharply as the number of points decreases, highlighting a key challenge for deploying LiDAR-guided RAFT-Stereo in practical, low-cost settings.

5 Sparse LiDAR-Guided RAFT-Stereo

The aforementioned performance degradation motivates us to analyze RAFT-Stereo in depth, aiming to recover the substantial gains enabled by dense LiDAR guidance.

5.1 Sparse guidance in the initial disparity map

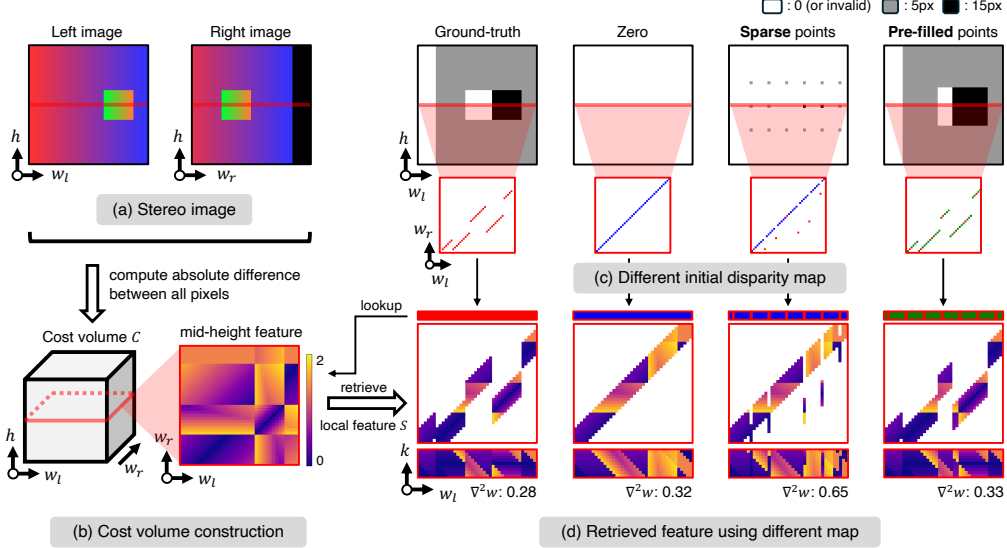
We first analyze how LiDAR-derived disparities in the initial disparity map influence RAFT-Stereo. As shown in Eq. (1), RAFT-Stereo uses previous disparity estimates as indices to retrieve *local* cost volume features for refining the estimates. This process can be interpreted as an *iterative local search* for the true disparity value at each pixel, making its performance likely sensitive to the initialization.

In the absence of prior information, RAFT-Stereo typically initializes with a zero disparity map, resembling an uninformed search. In contrast, LiDAR-derived disparities provide guidance for a more informed initialization, akin to an informed search.

The challenge, however, arises as LiDAR measurements become increasingly sparse. In such cases, naively injecting LiDAR-derived disparity values only into the corresponding pixels leaves large portions of the map still initialized with zero disparity, limiting the benefit of informed initialization. Upon closer inspection of RAFT-Stereo’s architecture, we further observe that its internal mechanisms may inadvertently suppress or ignore LiDAR guidance when input is extremely sparse.

Toy example. To illustrate this effect, we develop a toy example using a pair of synthesized images shown in Fig. 4a. The scene comprises a background and a foreground object, each exhibiting gradually changing colors—red to blue for the background and green to orange for the foreground. The true disparity values are 15 for the foreground and 5 for the background, as shown in Fig. 4c.

We first construct RAFT-Stereo’s cost volume, as shown in Fig. 4b, using the **L1 distance** between RGB pixel values instead of correlation to improve visualization clarity. We then retrieve cost volume features using different initial disparity maps, shown in Fig. 4c, resulting in different local regions S . Specifically, we consider four initialization strategies: the full ground-truth disparity map, a zero-



h : height of left/right images w_l : width of left image w_r : width of right image k : cost volume lookup range $\nabla^2 w$: Laplacian

Figure 4: Illustration of cost volume retrieval in RAFT-Stereo [1]. We compare four different initial disparity maps for feature retrieval: ground-truth disparity, default zero initialization, sparse ground truth *mimicking sparse LiDAR*, and a nearest-neighbor-filled version of the sparse map, as shown in (c). In (d), the retrieved features using the sparse ground truth exhibit unintended horizontal artifacts due to abrupt disparity changes, which limit the effectiveness of informed initialization. In contrast, pre-filling the missing disparities helps reinforce spatial consistency and better preserve useful guidance within the retrieved features.

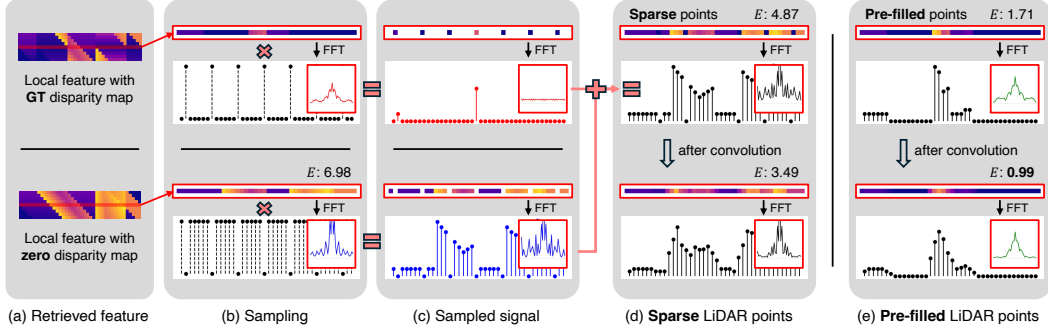


Figure 5: Analysis of cost volume features retrieved with sparse guidance. (a)-(d): The retrieved features using sparse disparity guidance (as in (d), top) can be viewed as a sampled combination of those obtained using ground-truth and zero-initialized maps (i.e., (a)-(c)). When the guidance is too sparse, the retrieved features are dominated by the zero-initialization, both before and after applying a low-pass filter—essentially burying useful information from sparse LiDAR points. (e): Pre-filling the missing disparity values enables effective guidance propagation. FFT: Fast Fourier Transform; E : L2 distance to features retrieved with the ground-truth map.

initialized map, a sparse ground-truth map *mimicking sparse LiDAR*, and a nearest-neighbor-filled version of the sparse map. For ease of visualization, we slice the 3D cost volume and the retrieved regions at the vertical midpoint, as shown in Fig. 4b (right) and at the bottom of Fig. 4d.

Sparse LiDAR points inject unintentional noise. While ground-truth disparities guide the retrieval of low-cost features (darker colors), sparsity introduces abrupt changes in the retrieved features, resulting in horizontal discontinuities. We quantify this spatial irregularity using the Laplacian $\nabla^2 w$, observing a much higher value for the sparse ground-truth than the full map (0.65 vs. 0.28).

We hypothesize that such spatial discontinuities act as noise, degrading RAFT-Stereo’s performance by making subsequent 2D convolutions for denoising and refinement more difficult. To test this, we conduct an experiment on KITTI, comparing a zero-initialized disparity map with and without added noise at every other pixel. As shown in Table 2, spatial noise in the initial disparity map—and thus in the retrieved features—leads to a measurable drop in RAFT-Stereo’s accuracy.

Table 2: **Spatial discontinuities in cost-volume retrieval degrade RAFT-Stereo.** We compare with and without noise in zero-initialized disparity maps.

Method	Noise	Bad1 (%)	Avg. Err. (px)
RAFT-Stereo [1]	✗	5.01	0.374
RAFT-Stereo [1]	✓	5.36	0.387

Table 3: **Performance of the two depth pre-fill methods alone,** before applying RAFT-Stereo on the pre-filled disparity maps.

Method	Bad1 (%)	Bad2 (%)	Avg. Err. (px)
IP-Basic [16]	52.51	37.71	2.772
Neural net	17.59	4.22	0.700

RAFT-Stereo struggles to propagate sparse guidance. One intuitive solution to this challenge is to propagate features retrieved via LiDAR guidance to nearby pixels, thereby reducing spatial discontinuities. At first glance, this could be achieved if RAFT-Stereo learns an effective low-pass filter to interpolate or diffuse the retrieved features. However, unlike conventional interpolation, the features at LiDAR-missing pixels are not zero-valued. Instead, even zero disparities retrieve features from the cost volume, as is standard in RAFT-Stereo. As a result, when LiDAR points are too sparse, their contributions are overwhelmed by features associated with zero disparities, causing the guided features to resemble high-frequency noise. Consequently, applying a low-pass filter fails to propagate the sparse guidance and instead attenuates it.

Fig. 5 illustrates this effect using the toy example, where the quality of the retrieved features is measured by their L2 distance to those obtained using the full ground-truth disparity map: a smaller distance indicates higher-quality retrieval. Panels (a)-(c) decompose the features retrieved under sparse guidance into components originating from the ground-truth and zero-disparity maps, along with their respective frequency responses. Panel (d) shows that, both before and after applying a low-pass filter, the retrieved features remain dominated by the zero-disparity component, which inadvertently suppresses the informative contributions from the sparse ground-truth/LiDAR points.

5.2 Depth pre-filling improves feature retrieval

To effectively leverage sparse LiDAR guidance without modifying the core architecture of RAFT-Stereo, we propose a *pre-densification step* to fill in missing disparity values. Namely, rather than relying on RAFT-Stereo to handle discontinuous features from sparse initial disparity maps, we smooth the disparity map in advance. This reduces horizontal discontinuities in the retrieved features while preserving LiDAR guidance. As shown in Fig. 4d, we apply nearest-neighbor interpolation to pre-fill LiDAR-missing pixels in the initial disparity map. This significantly reduces spatial discontinuity in the retrieved local region, lowering the Laplacian value $\nabla^2 w$ from 0.65 to 0.33. The effectiveness of this strategy is further illustrated in Fig. 5e, where the L2 distance of the retrieved features decreases sharply, indicating that the zero-disparity component no longer dominates feature retrieval.

What pre-filling method should we apply? Moving beyond the toy example to more realistic LiDAR guidance, a more sophisticated pre-filling method may be required. This problem is closely related to depth completion, where the goal is to predict a dense depth map from a sparse one, often using a monocular image as additional input. We explore two depth-completion methods:

- an image-processing-based interpolation method [16] (*i.e.*, IP-Basic), without the need to train a neural network;
- a more accurate approach based on a neural network (3.26M parameters), inspired by [55] (Fig. 6).

We fix the number of LiDAR points to 300 per frame, pre-train the neural network, and freeze it throughout the entire experiment. Fig. 2 shows examples of both methods.

Table 3 reports the disparity error of the pre-filling methods alone, while Table 4 presents the results of LiDAR-guided RAFT-Stereo, using the pre-filled initial disparity maps. We highlight two key observations. First, we observe that pre-filling the disparity map significantly boosts final

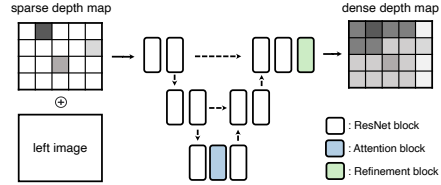


Figure 6: **The neural network architecture for depth pre-filling,** using non-local spatial propagation [55] for the refinement block.

Table 4: **Pre-filling the initial disparity map notably improves LiDAR-guided RAFT-Stereo.** We show the results by both the image processing-based [16] and neural network-based pre-filling.

Depth pre-fill	# Points	Bad1 (%)	Bad2 (%)	Avg. Err. (px)
① -	0	5.01	0.41	0.374
② -	300	4.32	0.37	0.359
③ IP-Basic [16]	Dense	3.61	0.36	0.310
④ Neural net	Dense	3.67	0.36	0.317

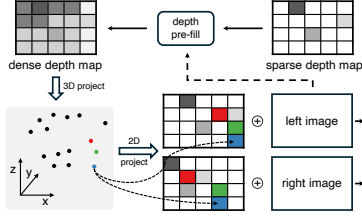


Figure 7: **Early fusion for enhanced cost volume.** Given the pre-filled depth map, we backproject pixels to 3D and reproject them into both images. Each 3D point’s XYZ is concatenated with RGB from the left/right image. This fused tensor—combining appearance and geometry—is passed to the feature encoder.

Table 5: **Incorporating LiDAR information via early fusion improves the LiDAR-guided RAFT-Stereo model introduced in Sec. 5.2.** Interestingly, while depth pre-filling yields additional gains, its underlying rationale differs fundamentally from that of densifying the initial disparity map—highlighting the need for a more accurate depth completion method. *: sampled from the pre-filled depth map.

	Feat. encoder	Depth pre-fill	# Points	Bad1 (%)	Avg. Err. (px)
①	Convolution	-	0	3.61	0.310
②	Convolution	-	300	3.51	0.299
③	Self-attention	-	0	3.56	0.304
④	Self-attention	-	300	3.41	0.297
⑤	Self-attention	IP-Basic [16]	Dense*	9.90	0.522
⑥	Self-attention	Neural net	1000*	3.33	0.294
⑦	Self-attention	Neural net	Dense*	3.44	0.300

performance (② vs. ③ & ④), demonstrating its effectiveness for LiDAR-guided RAFT-Stereo. Second, a more accurate depth completion method does not necessarily yield better performance (③ vs. ④). This suggests that even a less accurate pre-filling method can benefit RAFT-Stereo, likely because RAFT-Stereo’s iterative refinement can correct and improve upon the initial estimate.

5.3 Can we use sparse LiDAR guidance elsewhere?

In addition to improving cost volume retrieval, we investigate *how to construct a more accurate cost volume* by incorporating sparse LiDAR guidance—ideally with minimal modification to the RAFT-Stereo pipeline.

As shown in Eq. (2), RAFT-Stereo builds the cost volume via feature correlation, where, ideally, pixels corresponding to the same 3D point should exhibit high correlation. This motivates us to project each LiDAR point into both the left and right images, identify the corresponding pixels, and concatenate the LiDAR point’s 3D coordinates with the RGB values of those pixels. By reinforcing the correspondence between left and right images in this manner—assigning identical XYZ values to corresponding pixels—we inject geometric cues into the feature encoder, thereby guiding it to construct a more accurate cost volume.

Fig. 7 illustrates this idea. For pixels lacking a projected LiDAR point, we concatenate zero values in place of the missing 3D coordinates. We discuss depth pre-filling strategies later in this subsection.

Table 5 summarizes the experimental results. We begin with the LiDAR-guided RAFT-Stereo model introduced in Sec. 5.2, which uses an initial disparity map obtained via image-processing-based depth pre-filling [16]. First, we compare the default ResNet feature encoder using only image input against a variant that incorporates additional LiDAR information. As shown in Table 5 ① vs. ②, incorporating LiDAR points during feature encoding leads to a clear performance gain. Next, we investigate a Transformer-like feature encoder with self-attention [36], motivated by its stronger ability to capture global context. This change yields a further improvement, as shown in Table 5 ① vs. ③ and ② vs. ④.

Is pre-filling helpful? We now investigate whether densifying the LiDAR guidance can further improve the early fusion approach described above. Following Sec. 5.2, we consider both image-processing-based (*i.e.*, IP-Basic) and neural-network-based depth completion methods. In sharp contrast to the findings in Sec. 5.2, neither method improves stereo matching performance (Table 5 ⑤ & ⑦ vs. ④); in fact, IP-Basic pre-filling significantly increases disparity error.

We hypothesize that the effectiveness of depth pre-filling differs between late fusion and early fusion. In the late fusion case, the goal of pre-filling the initial disparity map is to retrieve informative and smooth cost volume features for iterative disparity refinement. In contrast, for early fusion, LiDAR guidance is injected into the input image space to explicitly indicate pixel correspondences—requiring much higher accuracy. As a result, inaccurate or overly smoothed depth completion can degrade performance rather than help.

To address this issue, we subsample the depth predictions from the completion network, retaining only the top-confidence pixels based on the prediction confidence from the final block (*i.e.*, the non-local spatial propagation block [55]). We find that retaining the top 1k depth-completed points yields further improvements in our final LiDAR-guided RAFT-Stereo (**GRAFT-Stereo**) model, which integrates both early and late fusion strategies.

Table 6: **Quantitative comparison to the SotA LiDAR-guided stereo methods on the KITTI Depth Completion dataset [14].** We train separate models, including the compared methods based on their official code for each guidance condition. GRAFT-Stereo consistently outperforms prior methods across various sparse LiDAR settings in depth metrics. gd: naive LiDAR-guidance; [†]: uniform sampling; [§]: beam sampling.

Method	300 points [†]	1000 points [†]	3000 points [†]	4-beam [§]	8-beam [§]	16-beam [§]
	RMSE / MAE	RMSE / MAE	RMSE / MAE	RMSE / MAE	RMSE / MAE	RMSE / MAE
EG-Depth [11]	829.7 / 283.6	822.6 / 263.0	764.0 / 242.5	900.0 / 307.3	851.2 / 277.8	858.9 / 276.7
SDG-Depth [12]	883.9 / 307.2	816.7 / 290.7	763.8 / 259.2	876.8 / 326.9	789.2 / 279.5	792.6 / 279.7
RAFT-Stereo [1] + gd	929.5 / 297.0	835.0 / 274.8	827.5 / 243.1	863.8 / 297.4	874.7 / 293.6	873.3 / 288.5
GRAFT-Stereo (Ours)	739.5 / 220.2	716.5 / 208.3	675.6 / 186.2	779.0 / 240.2	774.4 / 235.1	767.8 / 230.5

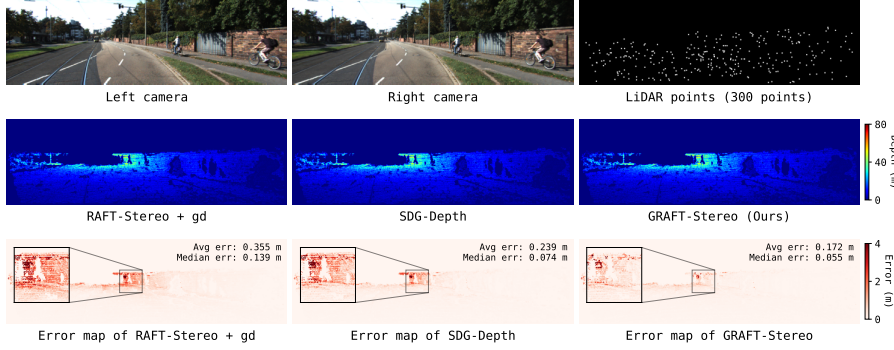


Figure 8: **Qualitative comparison of predicted depth maps.** GRAFT-Stereo produces more accurate depth than the baseline methods. Error maps are computed with respect to ground-truth. gd: naive LiDAR-guidance.

6 Additional Experiments and Analysis

Comparison to SotA LiDAR-guided methods. Beyond disparity estimation in Fig. 1b, we evaluate GRAFT-Stereo on the depth estimation task, by comparing it to representative LiDAR-guided stereo methods [11, 12]. For a fair comparison, we retrain the baselines using their official code, with separate models for each sparsity level. As shown in Table 6, our method consistently outperforms prior methods under sparse LiDAR input, across both uniform and beam sampling settings. A qualitative comparison in Fig. 8 further demonstrates that GRAFT-Stereo produces more accurate depth, especially at distant ranges, validating its effectiveness for both disparity and depth estimation.

Results on additional datasets. We further extend our evaluation to additional datasets, including VKITTI2 [17] and MS2 [18]. For fair comparison, we fine-tune all models on each dataset; please refer to the supplementary material for the detailed settings. As shown in Table 7, GRAFT-Stereo consistently outperforms the baseline methods across both datasets, highlighting the strength of RAFT-Stereo and the effectiveness of our approach in leveraging sparse guidance.

Additional empirical studies and qualitative results.

We leave additional results in the supplementary material, including experiments with 64-beam LiDAR, computation-accuracy trade-off, test-time robustness, mid-level fusion [46] and qualitative results.

Table 7: **Depth estimation results on VKITTI2 [17] and MS2 [18].** # Points: available LiDAR points per frame. GRAFT-Stereo surpasses other methods on both datasets, demonstrating its generalizability in leveraging sparse LiDAR points for guidance.

Dataset	Method	# Points	RMSE (mm)	MAE (mm)
VKITTI2	EG-Depth [11]	300	4437.8	927.5
	SDG-Depth [12]	300	3818.7	1187.7
	GRAFT-Stereo (Ours)	300	3761.7	877.5
MS2	EG-Depth [11]	300	1854.5	998.5
	SDG-Depth [12]	300	1471.1	843.3
	GRAFT-Stereo (Ours)	300	1465.9	781.4

7 Conclusion (limitations and broader impact discussed in the supplementary material)

We explore the use of LiDAR guidance in RAFT-Stereo, aiming to leverage extremely sparse yet accurate depth information to enhance stereo matching. Through a systematic investigation, we show that both early and late fusion can be effective—provided the sparse guidance is carefully integrated. A key insight from our study is that RAFT-Stereo’s internal mechanism tends to suppress the influence of sparse LiDAR input during late fusion. However, this limitation can be overcome by pre-filling the initial disparity map. By further combining this with early fusion, our LiDAR-guided RAFT-Stereo variant, **GRAFT-Stereo**, achieves state-of-the-art performance in stereo disparity estimation under sparse LiDAR conditions across various datasets.

Acknowledgment

This research is supported by grants from the Office of Naval Research (N6833523C0704). We are thankful for the generous support of the computational resources by the Ohio Supercomputer Center.

References

- [1] Lahav Lipson, Zachary Teed, and Jia Deng. Raft-stereo: Multilevel recurrent field transforms for stereo matching. In *3DV*, 2021.
- [2] Gangwei Xu, Xianqi Wang, Xiaohuan Ding, and Xin Yang. Iterative geometry encoding volume for stereo matching. In *CVPR*, 2023.
- [3] Xianqi Wang, Gangwei Xu, Hao Jia, and Xin Yang. Selective-stereo: Adaptive frequency information selection for stereo matching. In *CVPR*, 2024.
- [4] Jiankun Li, Peisen Wang, Pengfei Xiong, Tao Cai, Ziwei Yan, Lei Yang, Jiangyu Liu, Haoqiang Fan, and Shuaicheng Liu. Practical stereo matching via cascaded recurrent network with adaptive correlation. In *CVPR*, 2022.
- [5] Jia-Ren Chang and Yong-Sheng Chen. Pyramid stereo matching network. In *CVPR*, 2018.
- [6] Alex Kendall, Hayk Martirosyan, Saumitro Dasgupta, Peter Henry, Ryan Kennedy, Abraham Bachrach, and Adam Bry. End-to-end learning of geometry and context for deep stereo regression. In *ICCV*, 2017.
- [7] Gengshan Yang, Joshua Manela, Michael Happold, and Deva Ramanan. Hierarchical deep stereo matching on high-resolution images. In *CVPR*, 2019.
- [8] Zhaoshuo Li, Xingtong Liu, Nathan Drenkow, Andy Ding, Francis X Creighton, Russell H Taylor, and Mathias Unberath. Revisiting stereo depth estimation from a sequence-to-sequence perspective with transformers. In *ICCV*, 2021.
- [9] Weiyu Guo, Zhaoshuo Li, Yongkui Yang, Zheng Wang, Russell H Taylor, Mathias Unberath, Alan Yuille, and Yingwei Li. Context-enhanced stereo transformer. In *ECCV*, 2022.
- [10] Jaesung Choe, Kyungdon Joo, Tooba Imtiaz, and In So Kweon. Volumetric propagation network: Stereo-lidar fusion for long-range depth estimation. *RAL*, 2021.
- [11] Zhenyu Xu, Yuehua Li, Shiqiang Zhu, and Yuxiang Sun. Expanding sparse lidar depth and guiding stereo matching for robust dense depth estimation. *RAL*, 2023.
- [12] Ang Li, Anning Hu, Wei Xi, Wenxian Yu, and Danping Zou. Stereo-lidar depth estimation with deformable propagation and learned disparity-depth conversion. In *ICRA*, 2024.
- [13] Xiaoming Zhao, Weihai Chen, Xingming Wu, Peter CY Chen, and Zhengguo Li. Sparse lidar assisted self-supervised stereo disparity estimation. In *CCDC*, 2022.
- [14] Jonas Uhrig, Nick Schneider, Lukas Schneider, Uwe Franke, Thomas Brox, and Andreas Geiger. Sparsity invariant cnns. In *3DV*, 2017.
- [15] Andreas Geiger, Philip Lenz, and Raquel Urtasun. Are we ready for autonomous driving? the kitti vision benchmark suite. In *CVPR*, 2012.
- [16] Jason Ku, Ali Harakeh, and Steven L Waslander. In defense of classical image processing: Fast depth completion on the cpu. In *CRV*, 2018.
- [17] Yohann Cabon, Naila Murray, and Martin Humenberger. Virtual kitti 2. *arXiv preprint arXiv:2001.10773*, 2020.
- [18] Ukcheol Shin, Jinsun Park, and In So Kweon. Deep depth estimation from thermal image. In *CVPR*, 2023.
- [19] Ramin Zabih and John Woodfill. Non-parametric local transforms for computing visual correspondence. In *ECCV*, 1994.

- [20] Qingxiong Yang, Liang Wang, and Narendra Ahuja. A constant-space belief propagation algorithm for stereo matching. In *CVPR*, 2010.
- [21] Olga Veksler. Stereo correspondence by dynamic programming on a tree. In *CVPR*, 2005.
- [22] Qingxiong Yang, Liang Wang, Ruigang Yang, Henrik Stewénus, and David Nistér. Stereo matching with color-weighted correlation, hierarchical belief propagation, and occlusion handling. *TPAMI*, 2008.
- [23] Heiko Hirschmüller. Stereo processing by semiglobal matching and mutual information. *TPAMI*, 2007.
- [24] Fabio Tosi, Alessio Tonioni, Daniele De Gregorio, and Matteo Poggi. Nerf-supervised deep stereo. In *CVPR*, 2023.
- [25] Tianyu Chang, Xun Yang, Tianzhu Zhang, and Meng Wang. Domain generalized stereo matching via hierarchical visual transformation. In *CVPR*, 2023.
- [26] Philippe Weinzaepfel, Thomas Lucas, Vincent Leroy, Yohann Cabon, Vaibhav Arora, Romain Brégier, Gabriela Csurka, Leonid Antsfeld, Boris Chidlovskii, and Jérôme Revaud. Croco v2: Improved cross-view completion pre-training for stereo matching and optical flow. In *ICCV*, 2023.
- [27] Biyang Liu, Huimin Yu, and Guodong Qi. Graftnet: Towards domain generalized stereo matching with a broad-spectrum and task-oriented feature. In *CVPR*, 2022.
- [28] Junpeng Jing, Jiankun Li, Pengfei Xiong, Jiangyu Liu, Shuaicheng Liu, Yichen Guo, Xin Deng, Mai Xu, Lai Jiang, and Leonid Sigal. Uncertainty guided adaptive warping for robust and efficient stereo matching. In *ICCV*, 2023.
- [29] Chaoran Tian, Weihong Pan, Zimo Wang, Mao Mao, Guofeng Zhang, Hujun Bao, Ping Tan, and Zhaopeng Cui. Dps-net: Deep polarimetric stereo depth estimation. In *ICCV*, 2023.
- [30] Matteo Poggi and Fabio Tosi. Federated online adaptation for deep stereo. In *CVPR*, 2024.
- [31] Gangwei Xu, Yun Wang, Junda Cheng, Jinhui Tang, and Xin Yang. Accurate and efficient stereo matching via attention concatenation volume. *TPAMI*, 2023.
- [32] Luca Bartolomei, Matteo Poggi, Fabio Tosi, Andrea Conti, and Stefano Mattoccia. Active stereo without pattern projector. In *ICCV*, 2023.
- [33] Tongfan Guan, Chen Wang, and Yun-Hui Liu. Neural markov random field for stereo matching. In *CVPR*, 2024.
- [34] Xianda Guo, Chenming Zhang, Juntao Lu, Yiqi Wang, Yiqun Duan, Tian Yang, Zheng Zhu, and Long Chen. Openstereo: A comprehensive benchmark for stereo matching and strong baseline. *arXiv preprint arXiv:2312.00343*, 2023.
- [35] Guorun Yang, Hengshuang Zhao, Jianping Shi, Zhidong Deng, and Jiaya Jia. Segstereo: Exploiting semantic information for disparity estimation. In *ECCV*, 2018.
- [36] Alexey Dosovitskiy, Lucas Beyer, Alexander Kolesnikov, Dirk Weissenborn, Xiaohua Zhai, Thomas Unterthiner, Mostafa Dehghani, Matthias Minderer, Georg Heigold, Sylvain Gelly, et al. An image is worth 16x16 words: Transformers for image recognition at scale. In *ICLR*, 2021.
- [37] Haoliang Zhao, Huizhou Zhou, Yongjun Zhang, Jie Chen, Yitong Yang, and Yong Zhao. High-frequency stereo matching network. In *CVPR*, 2023.
- [38] Haoliang Zhao, Huizhou Zhou, Yongjun Zhang, Yong Zhao, Yitong Yang, and Ting Ouyang. Eai-stereo: Error aware iterative network for stereo matching. In *ACCV*, 2022.
- [39] Jiayi Zeng, Chengtang Yao, Lidong Yu, Yuwei Wu, and Yunde Jia. Parameterized cost volume for stereo matching. In *ICCV*, 2023.

- [40] Zachary Teed and Jia Deng. Raft: Recurrent all-pairs field transforms for optical flow. In *ECCV*, 2020.
- [41] Xuelian Cheng, Yiran Zhong, Yuchao Dai, Pan Ji, and Hongdong Li. Noise-aware unsupervised deep lidar-stereo fusion. In *CVPR*, 2019.
- [42] N-A-M Mai, Pierre Duthon, Louahdi Khoudour, Alain Crouzil, and Sergio A Velastin. Sparse lidar and stereo fusion (sls-fusion) for depth estimation and 3d object detection. In *ICPRS*, 2021.
- [43] Tsun-Hsuan Wang, Hou-Ning Hu, Chieh Hubert Lin, Yi-Hsuan Tsai, Wei-Chen Chiu, and Min Sun. 3d lidar and stereo fusion using stereo matching network with conditional cost volume normalization. In *IROS*, 2019.
- [44] Yongjian Zhang, Longguang Wang, Kunhong Li, Zhiheng Fu, and Yulan Guo. Slfnnet: A stereo and lidar fusion network for depth completion. *RAL*, 2022.
- [45] Andrea Pilzer, Yuxin Hou, Niki Loppi, Arno Solin, and Juho Kannala. Expansion of visual hints for improved generalization in stereo matching. In *WACV*, 2023.
- [46] Matteo Poggi, Davide Pallotti, Fabio Tosi, and Stefano Mattoccia. Guided stereo matching. In *CVPR*, 2019.
- [47] Yu-Kai Huang, Yueh-Cheng Liu, Tsung-Han Wu, Hung-Ting Su, Yu-Cheng Chang, Tsung-Lin Tsou, Yu-An Wang, and Winston H Hsu. S3: Learnable sparse signal superdensity for guided depth estimation. In *CVPR*, 2021.
- [48] Kihong Park, Seungryong Kim, and Kwanghoon Sohn. High-precision depth estimation with the 3d lidar and stereo fusion. In *ICRA*, 2018.
- [49] Junming Zhang, Manikandasriram Srinivasan Ramanagopal, Ram Vasudevan, and Matthew Johnson-Roberson. Listereo: Generate dense depth maps from lidar and stereo imagery. In *ICRA*, 2020.
- [50] Shreyas S Shivakumar, Ty Nguyen, Ian D Miller, Steven W Chen, Vijay Kumar, and Camillo J Taylor. Dfusenet: Deep fusion of rgb and sparse depth information for image guided dense depth completion. In *ITSC*, 2019.
- [51] Jiaxiong Qiu, Zhaopeng Cui, Yinda Zhang, Xingdi Zhang, Shuaicheng Liu, Bing Zeng, and Marc Pollefeys. Deeplidar: Deep surface normal guided depth prediction for outdoor scene from sparse lidar data and single color image. In *CVPR*, 2019.
- [52] Mu Hu, Shuling Wang, Bin Li, Shiyu Ning, Li Fan, and Xiaojin Gong. Penet: Towards precise and efficient image guided depth completion. In *ICRA*, 2021.
- [53] Jie Tang, Fei-Peng Tian, Wei Feng, Jian Li, and Ping Tan. Learning guided convolutional network for depth completion. *TIP*, 2020.
- [54] Lina Liu, Xibin Song, Jiadai Sun, Xiaoyang Lyu, Lin Li, Yong Liu, and Liangjun Zhang. Mff-net: Towards efficient monocular depth completion with multi-modal feature fusion. *RAL*, 2023.
- [55] Jinsun Park, Kyungdon Joo, Zhe Hu, Chi-Kuei Liu, and In So Kweon. Non-local spatial propagation network for depth completion. In *ECCV*, 2020.
- [56] Sifei Liu, Shalini De Mello, Jinwei Gu, Guangyu Zhong, Ming-Hsuan Yang, and Jan Kautz. Learning affinity via spatial propagation networks. In *NeurIPS*, 2017.
- [57] Xinjing Cheng, Peng Wang, and Ruigang Yang. Depth estimation via affinity learned with convolutional spatial propagation network. In *ECCV*, 2018.
- [58] Yufei Wang, Bo Li, Ge Zhang, Qi Liu, Tao Gao, and Yuchao Dai. Lrru: Long-short range recurrent updating networks for depth completion. In *ICCV*, 2023.

- [59] Lina Liu, Xibin Song, Xiaoyang Lyu, Junwei Diao, Mengmeng Wang, Yong Liu, and Liangjun Zhang. Fcfr-net: Feature fusion based coarse-to-fine residual learning for depth completion. In *AAAI*, 2021.
- [60] Kaiming He, Xiangyu Zhang, Shaoqing Ren, and Jian Sun. Deep residual learning for image recognition. In *CVPR*, 2016.
- [61] Yurong You, Yan Wang, Wei-Lun Chao, Divyansh Garg, Geoff Pleiss, Bharath Hariharan, Mark Campbell, and Kilian Q Weinberger. Pseudo-lidar++: Accurate depth for 3d object detection in autonomous driving. *ICLR*, 2020.
- [62] Yihan Wang, Lahav Lipson, and Jia Deng. Sea-raft: Simple, efficient, accurate raft for optical flow. In *ECCV*, 2024.
- [63] Yiming Zhao, Lin Bai, Ziming Zhang, and Xinming Huang. A surface geometry model for lidar depth completion. *RAL*, 2021.
- [64] Yingxiang Li, Yingke Gao, Zhiwen Su, Shitao Chen, and Longjun Liu. Fpga accelerated real-time recurrent all-pairs field transforms for optical flow. In *CAC*, 2022.
- [65] Ye Liu, Shuang Hao, Kun Huang, Minghui Yang, Zili Huang, Xiuyuan Qi, Yiting Li, Liang Zhou, Yu Long, and Jun Zhou. An fpga-based ultra-high performance and scalable optical flow hardware accelerator for autonomous driving. In *ISCAS*, 2024.

Supplementary Material for **Leveraging Sparse LiDAR for RAFT-Stereo: A Depth Pre-Fill Perspective**

In this supplementary material, we provide additional details omitted in the main paper.

- Sec. S1: Discussion of limitations and broader societal impact.
- Sec. S2: Additional implementation details.
- Sec. S3: Extended analysis and experimental results.

S1 Discussion

S1.1 Limitations

In the main paper, we have explored the use of sparse LiDAR points to effectively guide RAFT-Stereo with minimal architectural modifications, and proposed **GRAFT-Stereo**, which achieves superior disparity and depth estimation performance compared to baseline LiDAR-guided stereo methods. However, several directions remain for future exploration. First, while we adopt RAFT-Stereo’s original disparity loss, incorporating more sophisticated depth losses may provide stronger supervision during training. Second, enhancing temporal consistency across frames using the provided sparse LiDAR guidance is a promising direction. We leave these for future work.

S1.2 Broader Impact

This paper explores the use of sparse yet accurate LiDAR points for stereo depth estimation, aiming to improve the practicality of depth perception systems in real-world scenarios. By effectively leveraging sparse LiDAR as guidance, our approach has the potential to enhance the 3D understanding of visual perception models while reducing reliance on costly sensor inputs. To the best of our knowledge, at the current stage, our work does not introduce any additional negative societal impacts compared to existing LiDAR-guided stereo depth estimation methods.

S2 Additional Implementation Details

We build our model on top of RAFT-Stereo [1]. The model is trained for 100k iterations using a learning rate of 2×10^{-3} with one-cycle decay. We set the batch size per GPU to 4 and use two NVIDIA A100 GPUs for all experiments. For the analysis in Sec. 5.2 of the main paper, we randomly crop the input images to a size of 336×1120 . In Sec. 5.3, we reduce the crop size to 224×784 due to GPU memory constraints. We train our model using a sequential L1 loss, following existing iterative methods [1, 3]. Specifically, our loss function is defined as:

$$L = \sum_{i=1}^N \alpha^{N-i} \|D_i - D_{gt}\|_1, \quad (\text{S1})$$

where α is the loss weight for each iteration, N is the number of refinement steps, and D_i and D_{gt} denote the estimated disparity map at iteration i and the ground-truth disparity map, respectively. We set $\alpha = 0.9$, and use $N = 22$ during training and $N = 32$ at test time.

For training the neural network-based depth pre-filling model in our study, we follow the objective function ($N = 1$) and hyperparameters used in training GRAFT-Stereo, with the exception that the ground-truth signal is the depth map instead of the disparity map. The pre-filling network is pretrained prior to GRAFT-Stereo using 300 LiDAR points and is kept frozen across all experiments, including those with varying LiDAR sparsity conditions.

To synthesize low-beam LiDAR, we follow the implementation provided by [63] and sample more LiDAR lines from the lower part of the scene, similar to the strategy used in [61].

Table S1: **Detailed quantitative comparison on disparity metrics with state-of-the-art LiDAR-guided stereo methods on the KITTI Depth Completion dataset [14].** We train separate models, including the compared methods based on their official code for each guidance condition. GRAFT-Stereo consistently outperforms prior methods across various sparse LiDAR settings in depth metrics. GRAFT-Stereo (late only) refers to our model that incorporates only improved disparity map initialization (Sec. 5.2), while GRAFT-Stereo (full) denotes the complete model with additional early feature fusion (Sec. 5.3). gd: naive LiDAR-guidance; \dagger : uniform sampling; \S : beam sampling.

Method	300 points \dagger	1000 points \dagger	3000 points \dagger	4-beam \S	8-beam \S	16-beam \S
	Avg. Err. / Bad1	Avg. Err. / Bad1	Avg. Err. / Bad1	Avg. Err. / Bad1	Avg. Err. / Bad1	Avg. Err. / Bad1
EG-Depth [11]	0.349 / 4.24	0.331 / 4.02	0.322 / 3.97	0.364 / 4.57	0.339 / 4.12	0.333 / 4.09
SDG-Depth [12]	0.381 / 5.33	0.369 / 4.82	0.349 / 4.48	0.388 / 5.10	0.355 / 4.52	0.347 / 4.36
RAFT-Stereo [1] + gd	0.359 / 4.32	0.334 / 3.84	0.309 / 3.50	0.365 / 4.65	0.359 / 4.53	0.359 / 4.53
GRAFT-Stereo (late only)	0.310 / 3.61	0.286 / 3.32	0.273 / 3.19	0.338 / 4.37	0.325 / 4.19	0.320 / 4.11
GRAFT-Stereo (full)	0.294 / 3.33	0.285 / 3.16	0.264 / 2.96	0.327 / 4.14	0.319 / 4.05	0.315 / 4.03

Toy example in Fig. 4 of the main paper. We synthesize a 40×40 stereo image pair by gradually interpolating two colors for the background and foreground. The foreground object has a size of 15×15 , and the ground-truth disparities are set to 6 and 15 pixels for the background and foreground, respectively. To simulate sparse LiDAR points, we horizontally sample every sixth pixel from the ground-truth disparity map.

Baseline methods in Fig. 1b and Table 6 of the main paper. For a fair comparison with baseline methods, we separately retrain RAFT-Stereo [1] (with naive guidance), EG-Depth [11], and SDG-Depth [12] under each sparse LiDAR guidance condition, using their official implementations and configurations.

Fine-tuning in Table 7 of the main paper. Virtual KITTI2 [17] is a synthetic dataset that provides dense ground-truth depth maps. Following the split strategy in [10], we utilize “Scene01” and “Scene02” for fine-tuning, while the remaining scenes serve as the test set. This results in 680 training frames and 1,446 testing frames. Similar to the sparse setting for KITTI Depth Completion [14], we randomly sample 300 points from the dense depth maps for fine-tuning. SDG-Depth [12] is fine-tuned for 5,000 steps with a learning rate of 3×10^{-4} and batch size of 4. EG-Depth [11] is fine-tuned for 20 epochs with a learning rate of 1×10^{-4} and batch size of 8.

MS2 [18] is a large-scale multi-spectral stereo dataset captured in real-world driving environments. It includes stereo images, raw LiDAR points, and semi-dense ground-truth depth maps. Due to the presence of repetitive scenes in the dataset, we adopt the same training and validation splits as [12]. Specifically, we select four sequences for training (“2021-08-06-11-23-45”, “2021-08-13-16-14-48”, “2021-08-13-16-31-10”, “2021-08-13-17-06-04”) and one for validation (“2021-08-13-16-08-46”), resulting in 10,120 training frames and 1,272 validation frames. We also fine-tune with randomly sampling 300 LiDAR points. SDG-Depth [12] is fine-tuned for 5,000 iterations with a learning rate of 3×10^{-4} , while EG-Depth [11] is fine-tuned with a learning rate of 1×10^{-4} . The batch size is set to 8 for both models.

S3 Additional Analysis and Experimental Results

Detailed quantitative results on disparity metrics. Table S1 reports the detailed numerical results on disparity metrics omitted from the main paper. For fair comparison, all baseline models are retrained using their official implementations. As shown in the table and in Fig. 1b, GRAFT-Stereo consistently outperforms baseline methods across various sparse LiDAR guidance conditions, demonstrating its broad applicability to LiDAR-guided stereo depth estimation under diverse sparse input conditions.

In addition, we report the performance of two variants of GRAFT-Stereo: a *late fusion only* model that uses improved disparity map initialization by IP-Basic [16] (denoted as GRAFT-Stereo (late only) in Table S1; Sec. 5.2), and the *full* model that additionally incorporates early feature fusion and a transformer-based encoder for enhanced cost volume construction (GRAFT-Stereo (full) in Table S1; Sec. 5.3). We find that the late fusion only model consistently improves upon RAFT-Stereo [1] with naive guidance, and that early fusion further boosts performance consistently.

Analysis on recurrent iterations and runtime. As discussed in the main paper, RAFT-Stereo [1] offers the flexibility of *anytime prediction*—producing less accurate depth under limited computational

Table S2: **Comparison with state-of-the-art LiDAR-guided stereo methods on the KITTI Depth Completion dataset [14] under the 64-beam LiDAR setting.** # Points indicates the number of LiDAR points available per frame. GRAFT-Stereo demonstrates competitive performance under the 64-beam setting, indicating its general applicability. gd: naive guidance.

Method	# Points	RMSE (mm)	MAE (mm)	Bad1 (%)	Avg. Err (px)
EG-Depth [11]	64-beam	675.5	197.2	3.68	0.302
SDG-Depth [12]	64-beam	623.2	197.6	3.60	0.300
RAFT-Stereo [1] + gd	64-beam	768.7	228.6	4.12	0.317
GRAFT-Stereo (Ours)	64-beam	685.4	193.0	4.12	0.306

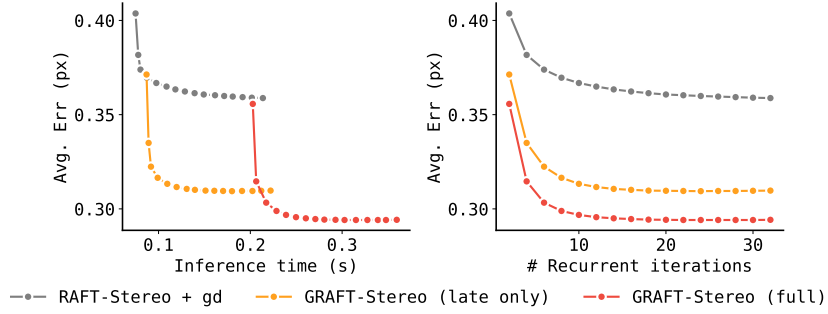


Figure S1: **Computation and accuracy trade-off during test time.** We compare accuracy and inference time by varying the number of recurrent iterations. GRAFT-Stereo (late only) refers to our variant that uses a ResNet [60]-based feature encoder and excludes early feature fusion (*i.e.*, Sec. 5.2). GRAFT-Stereo (full) denotes the complete model with both early and late fusion, as well as a transformer [36]-based encoder (*i.e.*, Sec. 5.3). Our GRAFT-Stereo variants provide a broad range of speed–accuracy trade-offs.

budgets and progressively refining it as more time becomes available. In Fig. S1, we illustrate the trade-off between accuracy and inference time by varying the number of recurrent iterations. We compare three models: RAFT-Stereo [1] with naive LiDAR guidance, GRAFT-Stereo with *late fusion only* (Sec. 5.2), and the *full* GRAFT-Stereo model with both early and late fusion (Sec. 5.3). We include the CPU runtime of IP-Basic [16] for image-processing-based depth pre-filling, since it is a CPU-only method. We note that the late fusion-only variant is fully convolutional, using a ResNet [60]-based feature encoder. Together with the previous observations from Table S1, we find that while all models benefit from additional recurrent iterations, our GRAFT-Stereo variants offer a wide range of speed–accuracy trade-offs, with the full model achieving the best overall performance.

While the above results are obtained using a GPU (NVIDIA A100), the model can be further optimized for real-world deployment on edge devices. For instance, FPGAs can run models with low delay and high energy efficiency by using parallel and pipelined execution [64, 65]. These features allow GRAFT-Stereo to keep its strong performance while running faster and using less power, making it a good fit for embedded systems, for example, self-driving cars or robots.

Comparison under 64-beam LiDAR settings. While the primary goal of our study is to leverage sparse—and thus more affordable—LiDAR to guide RAFT-Stereo [1], we also evaluate our method under the 64-beam LiDAR setting. As shown in Table S2, GRAFT-Stereo achieves competitive performance across both disparity and depth metrics, comparable to existing state-of-the-art methods. This demonstrates that GRAFT-Stereo remains effective even under high-density LiDAR configurations.

Analysis on mid fusion with GSM [46]. We investigate whether cost volume adjustment via mid fusion can further improve performance under extremely sparse LiDAR input. Specifically, we apply Guided Stereo Matching [46] at test time. Consistent with the findings in [32], the results in Table S3 show that neither the sparse points nor the densified depth maps lead to noticeable improvement.

Analysis on the number of points during test time. To evaluate the robustness of GRAFT-Stereo with respect to the number of LiDAR points at test time, we experiment with varying point densities using a model trained on 300 LiDAR points. As shown in Fig. S2, performance improves up to 1,500 points, demonstrating robustness, but degrades when the number becomes excessively large.

Table S3: **Analysis on mid fusion with GSM [46].** Cost volume adjustment doesn’t bring performance improvement together with GRAFT-Stereo. *: sampled from the pre-filled depth map.

GSM [46]	Depth Pre-fill	# Points	Bad1 (%)	Avg. Err (px)
✗	-	-	3.33	0.294
✓	-	300	3.45	0.299
✓	IP-Basic [16]	30000*	3.37	0.296
✓	IP-Basic [16]	Dense*	11.71	0.684
✓	Neural net	30000*	3.33	0.294
✓	Neural net	Dense*	11.59	0.670

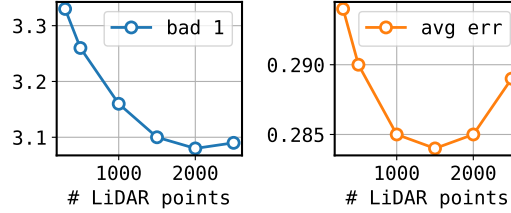


Figure S2: **Effect of the number of LiDAR points during test time.** We use GRAFT-Stereo trained with 300 LiDAR points and vary the number of points during inference. Performance improves with more LiDAR points, demonstrating robustness, but degrades when too many points are provided.

Qualitative comparison. In Fig. S3, we qualitatively compare disparity errors across RAFT-Stereo [1], RAFT-Stereo with naive LiDAR guidance (*i.e.*, directly using sparse LiDAR points as an initial map), and our proposed GRAFT-Stereo. We observe that both RAFT-Stereo and the naive guidance baseline often produce overly smooth or noisy predictions, whereas GRAFT-Stereo produces more accurate and detailed disparity maps using only a few hundred points.

In Fig. S4 and Fig. S5, we provide additional qualitative results on depth errors under different sparse LiDAR conditions, including uniformly sampled 300 LiDAR points and synthesized 4-beam LiDAR. As shown, GRAFT-Stereo consistently produces more accurate dense depth maps than baseline methods, demonstrating its effectiveness across various sparse LiDAR settings.

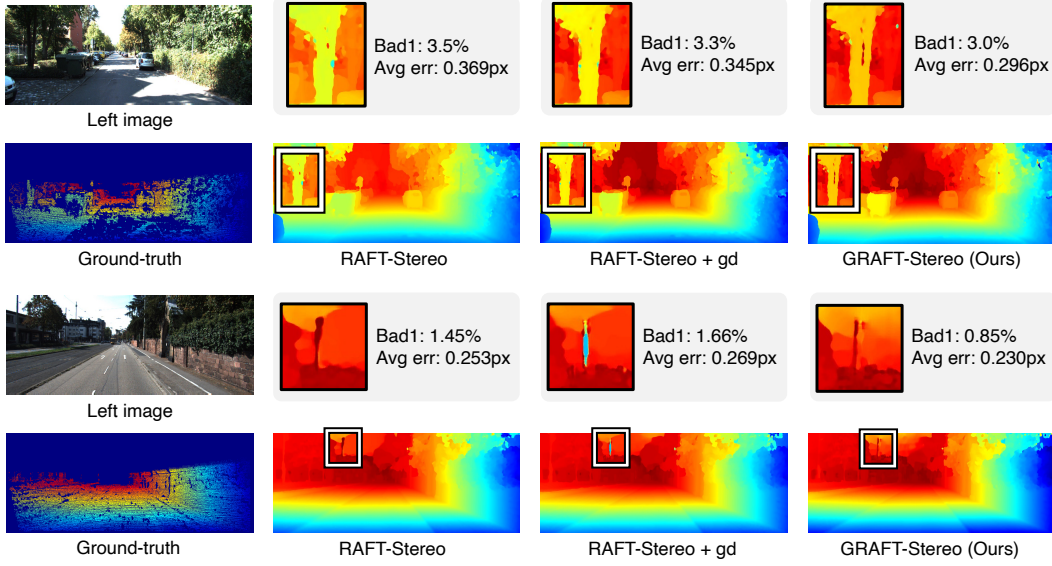


Figure S3: **Qualitative results on disparity estimation demonstrating improvements over RAFT-Stereo [1].** GRAFT-Stereo produces sharper and more detailed disparity maps compared to the baselines. Both RAFT-Stereo + naive guidance and GRAFT-Stereo are trained using 300 LiDAR points. gd: naive LiDAR-guidance.

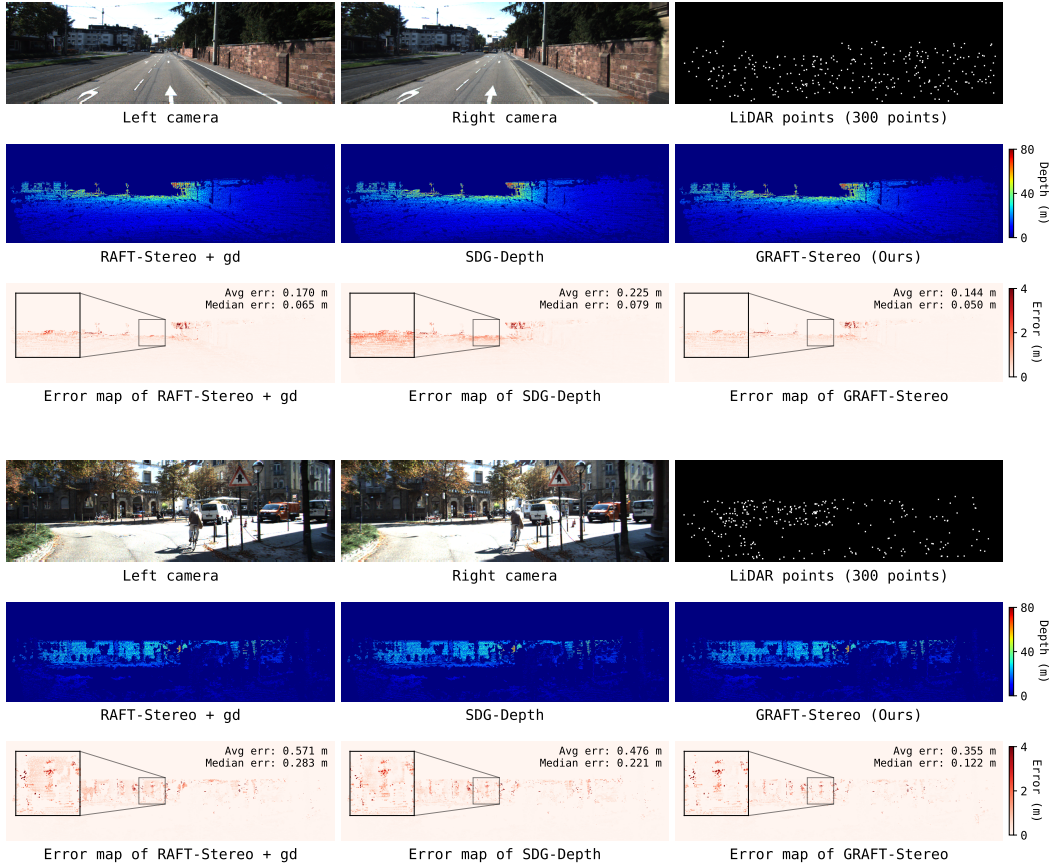


Figure S4: **Additional qualitative comparison of predicted depth maps with 300 LiDAR points.** GRAFT-Stereo produces more accurate depth predictions than the baseline methods. Error maps are computed with respect to ground-truth. gd: naive LiDAR-guidance.

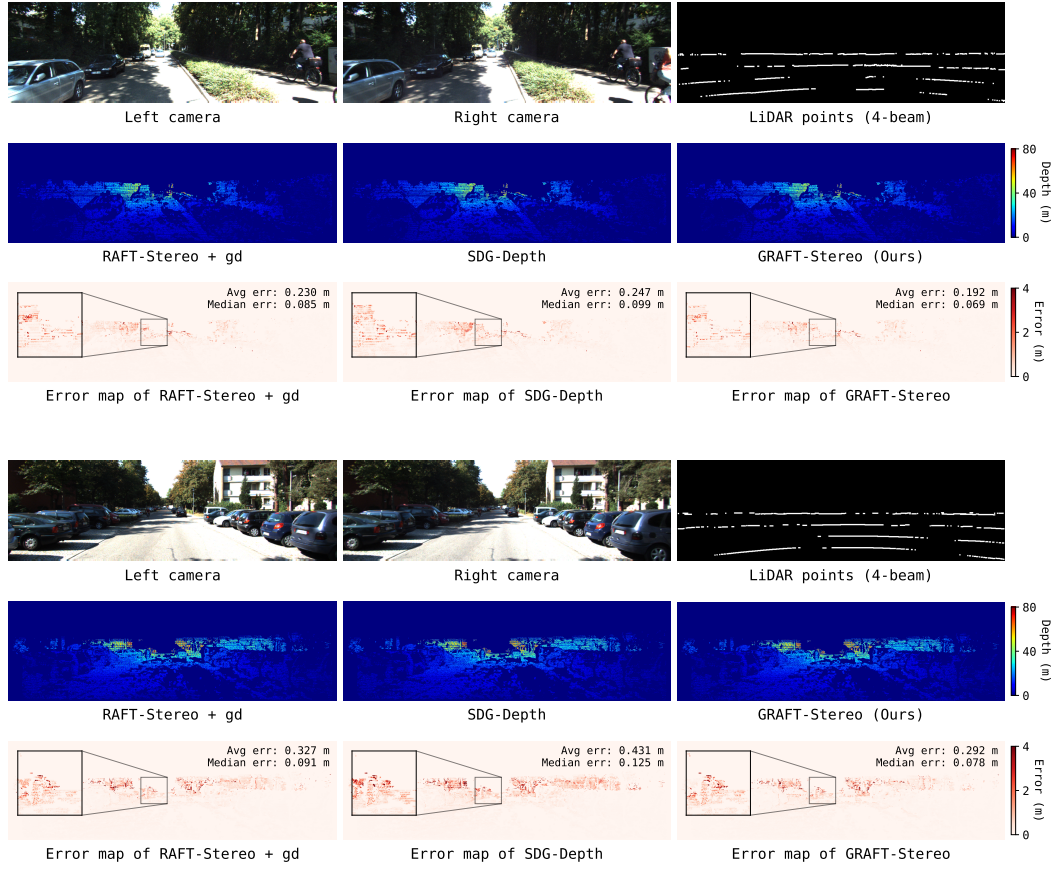


Figure S5: **Additional qualitative comparison of predicted depth maps with 4-beam LiDAR.** GRAFT-Stereo produces more accurate depth predictions than the baseline methods. Error maps are computed with respect to ground-truth. gd: naive LiDAR-guidance.